JOURNAL OF NANOSCIENCE LETTERS

Control of rotary motion at the nanoscale: Motility, actuation, self-assembly

Petr Král[*,†], Lela Vuković, Niladri Patra, Boyang Wang, Kyaw Sint, Alexey Titov

Department of Chemistry, University of Illinois at Chicago, Chicago, IL 60607, USA
† Dedicated to my father, Salamoun Klein, a Holocaust survivor

[*]Author for correspondence: Petr Král, email: pkral@uic.edu
Received 20 Dec 2010; Accepted 9 Feb 2011; Available Online 20 Apr 2011

Abstract

Controlling motion of nanoscale systems is of fundamental importance for the development of many emerging nanotechnology areas. We review a variety of mechanisms that allow controlling rotary motion in nanoscale systems with numerous potential applications. We discuss control of rotary motion in molecular motors, molecular propellers of liquids, nanorods rolling on liquids, nanochannels with rotary switching motion, and self-assembly of functional carbonaceous materials, guided by water nanodroplets and carbon nanotubes.

Keywords: Rotary motion; Molecular motor; Molecular propeller; Nanopore; Nanochannels; Self-assembly

1. Introduction

Rotary and cyclic motions provide motility to biological systems at different length scales. For example, flagella [1] and cilia [2] can rotate and beat, respectively, to propel bacteria. Their motion is powered by molecular motors. The molecular motor F_1F_0-ATP synthase, schematically shown in Figure 1, synthesizes ATP during rotation powered by proton flow [3]. The proton concentration gradient across the membrane causes protons to pass through the F_0 unit, thereby rotating it. F_0 drives the central stalk of the F_1 unit, blocked from rotation by the side paddle. The rotation of the central stalk inside F_1 causes the synthesis of ATP. Alternatively, ATP can be consumed to power rotary molecular motors based on the F_1 unit. Cells can also transport molecules and micelles [4] by other molecular motors, such as kinesin

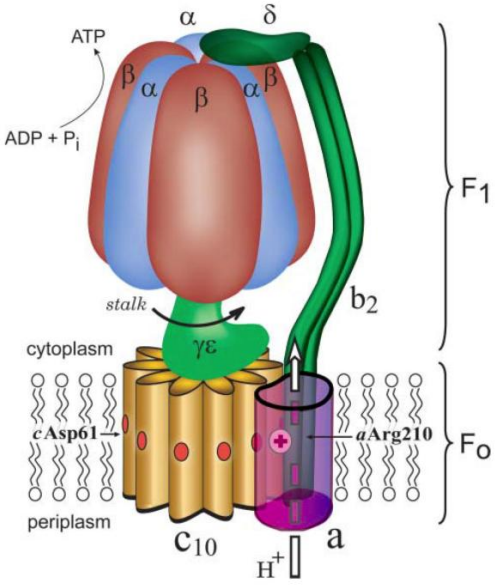

Figure 1. The F_1F_0-ATP synthase is formed by F_0 and F_1 units. F_0 is inside and F_1 is outside the membrane. Reprinted from [3], Biophysical Journal, 86 / 3, A. Aksimentiev, I. A. Balabin, R. H. Fillingame, K. Schulten, *Insights into the Molecular Mechanism of Rotation in the F_0 Sector of ATP Synthase*, 1332-1344, Copyright (2004), with permission from Elsevier.

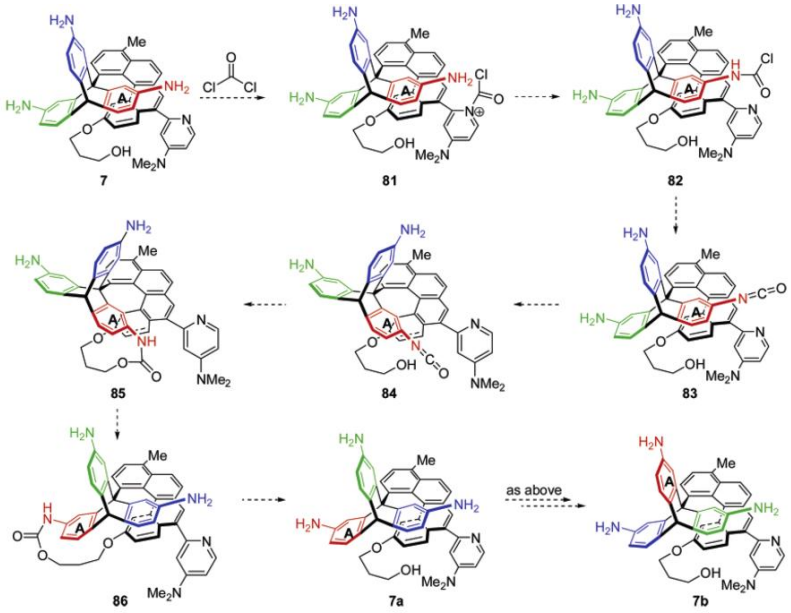

Figure 2. Steps of the rotation of a chemically powered molecular motor. Reprinted with permission from [36] Copyright 2007 American Chemical Society.

[5], dynein [6], and myosin [7], which move molecular cargo along tubulous filaments.

The realization and control of rotary motion at the nanoscale is of great importance in synthetic nanosystems. First attempts to achieve this goal were based on hybrid systems combining the existing natural molecular machinery with synthetic components. In this approach, transport of nanoparticles and other molecular cargo by molecular motors has been successfully tested [8–10]. The synthetic components need to be based on durable materials with excellent mechanical and chemical properties [11]. For example nanocarbons, such as carbon nanotubes (CNT), nanocones, and graphene [12–14], have many unique properties that make them ideal for the fabrication of active nanoscale components. They are chemically stable, very strong and rigid, since covalent binding of their carbon atoms is realized by planar sp2-orbitals. They can be modified by physisorption [15], doping [16], and chemical functionalization [17–22].

For example, nanoscale metal plates can rotate around multiwalled CNTs, when driven by time-dependent electric field, similar to molecular rotors [23, 24]. Their motion is possible due to the low static intershell friction between the CNTs. Electrons flowing through a chiral CNT inserted into a larger CNT could set it into rotational motion [25].

In this review, we explore the possibilities for controlling rotary motion in nanoscale systems, such as molecular motors, propellers, channels, and other nanostructures. We discuss potential applications of these hybrid systems.

2. Motility at the nanoscale

2.1. Molecular motors

In order to power nanoscale machines, we first need to design and synthesize robust molecular motors. Synthetic molecular motors could be driven by optical [26–30], electrical [31], chemical [32], thermal [33], and other (ratchet-like) means [34, 35].

For example, Kelly *et al.* rationally designed and synthesized a chemically-powered rotary molecular motor, seen in Figure 2 [36]. Feringa *et al.* synthesized light-driven rotary molecular motors having 4 reaction steps in each rotation cycle, as shown in Figure 3 (top) [37]. This molecular motor was incorporated into molecular nanocars with fullerene wheels that can be translated on gold surfaces upon optical excitation, presented in Figure 3 (middle and bottom) [38, 39]. Molecular rotors, such as hexa-ter-butyldecacyclene, spontaneously rotate on material surfaces [40]. Grill *et al.* drove by a STM tip the rotation of a single molecule on the material surface [41].

In 1748, Benjamin Franklin invented "electric wheel," shown in Figure 4 (top) [42], and ever since electric driving became the most efficient way of powering motors [43]. Franklin's motor consisted of a vertical shaft that was free to rotate, from which several glass bars extended like spokes. Each bar was tipped with a brass thimble. Placing the terminal of a negatively charged Leyden jar near the wheel allowed the thimble/glass assemblies to act as

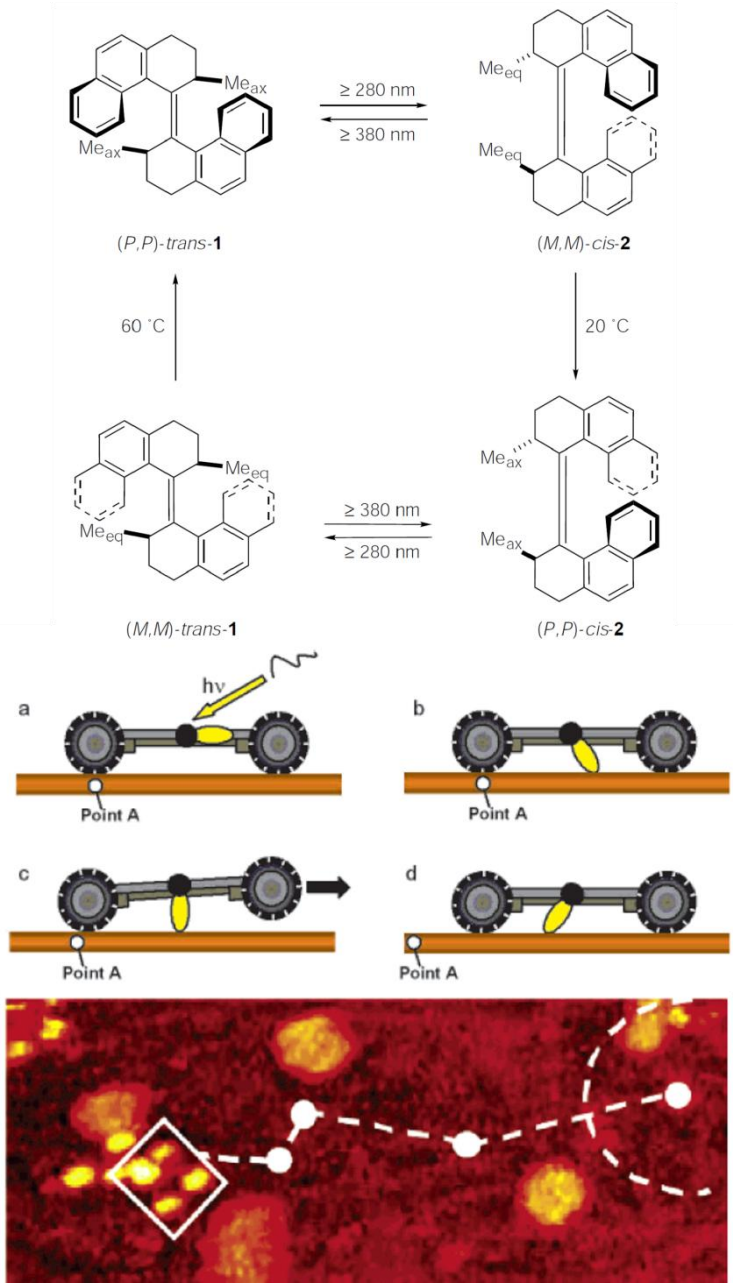

Figure 3. (top) Rotary cycle of the light-driven rotary molecular motor. Reprinted by permission from Macmillan Publishers Ltd: Nature [37], copyright (1999). (middle) Principal of optical excitation and related motion of the nanocar. Reprinted with permission from [38]. Copyright 2006 American Chemical Society. (bottom) Trajectory of the nanocar driven by light. Reprinted with permission from [39]. Copyright 2005 American Chemical Society.

capacitors; as each assembly charged up, it tended to be repelled from the Leyden jar. A second, positively charged jar set nearby had the opposite effect, pulling the spokes towards it. The result was that the wheel would begin to rotate, and it would remain in motion until the charges on the Leyden jars dissipated.

Electronic driving of synthetic molecular motors could be achieved by passing electric current through a helical molecule [31]. Rapenne *et al.* synthesized a molecular motor with a rotor and a stator designed in a similar way as Franklin's motor, as seen in Figure 4 (bottom) [44, 45]. To make nanoscale analogs of Franklin's motor active, one needs to charge the blades. This can be done by electron tunneling, which can induce periodic vibrational [46] and translational motion in molecules [47]. Here, we show how nanoscale vibrations can be effectively transformed into concerted rotary motion by electron tunneling [48].

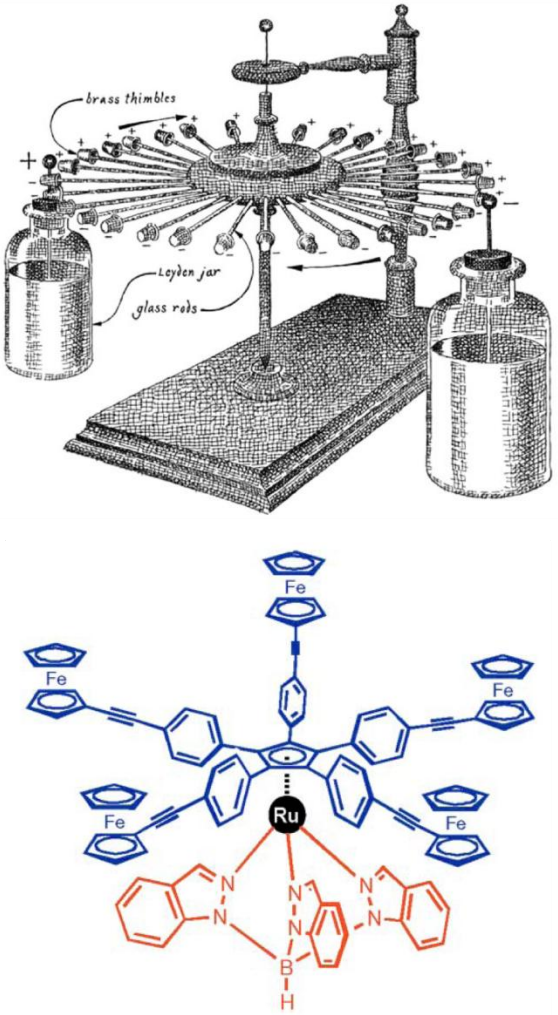

Figure 4. (top) Franklin's electric motor [42] - reproduced by permission of The Royal Society of Chemistry. (bottom) Structure of the active part of a single-molecular motor. The lower ligand is the stator and the upper ligand is the rotor with five ferrocene-terminated arms. The ruthenium plays the role of joint between the two ligands [44] - reproduced by permission of The Royal Society of Chemistry.

In Figure 5 (top), we present two types of proposed electron tunneling-driven molecular motors, made with three (left) and six (right) stalks [48]. Their shaft is formed by a (12,0) carbon nanotube (CNT) [49], which could be mounted into CNT bearings [50]. The stalks are formed by polymerized iceane molecules with saturated bonds [51], attached to the shaft at an angle of 120° or 60° with respect to each other. The length of stalks was chosen to prevent non-resonant electron tunneling from the blades to the shaft [52]. The energies of their electronic states should also prevent the electron transfer along the stalks by resonant tunneling [53]. The blades are made of molecules with conjugated bonds (fullerenes) covalently attached at the top of the stalks. In our MD simulations, an external homogeneous electrostatic field E, oriented along the vertical z direction, has been used for periodical charging and discharging of the blades by electron tunneling from two neutral electrodes, placed and immobilized in the proximity of the motor, as shown in Figure 5 (top). The field E powers the system by rotating the formed dipole p of the rotor that is on average orthogonal to the field direction. Once the dipole is formed with one of the two orientations, it is unidirectionally rotated by the electric field.

In Figure 5 (bottom), we show the efficiency of these electron tunneling-driven motors obtained by applying different damping torques to the motors. In the limit of high damping torque (high loading), the efficiency saturates to $\eta \sim 0.85$ and $\eta \sim 0.6$ for the three- and six-fullerene motors, respectively. The maximum efficiency of the motors, $\eta = 1$, is never observed due to dissipation of the angular momentum of the motors to their internal phonon modes. For lower damping (loading), the

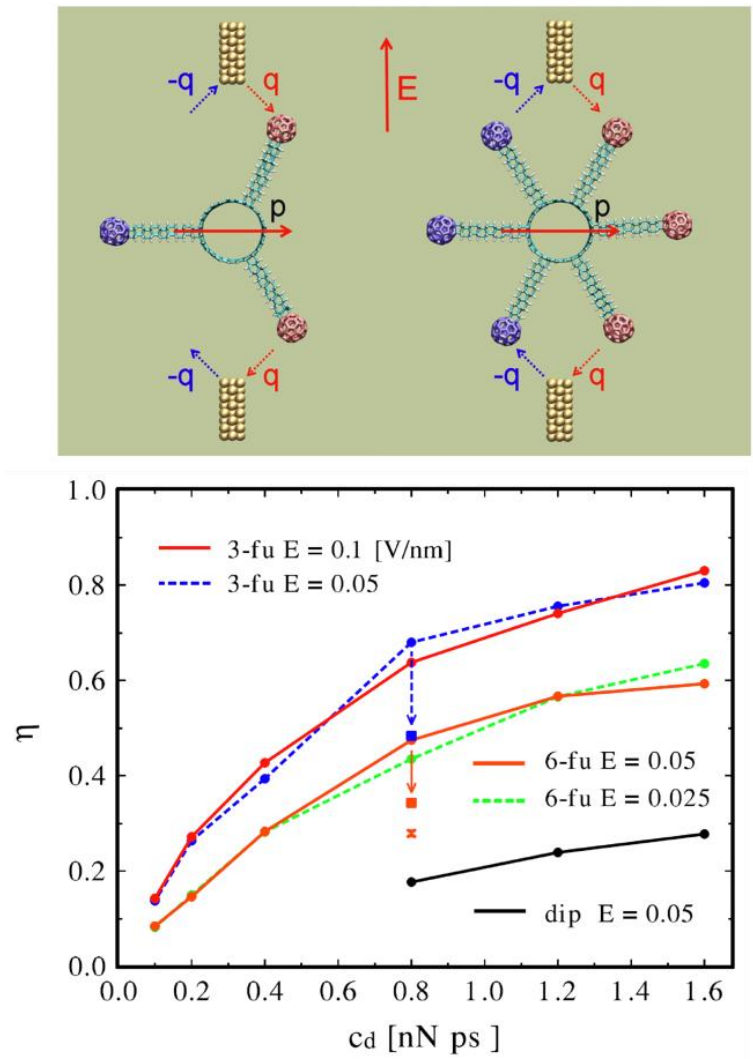

Figure 5. (top) Electron tunneling-driven nanoscale motors with three (left) and six (right) fullerene blades. (bottom) Dependence of the efficiency η for the 3-fullerene and 6-fullerene motors on the damping coefficient c_d. At larger c_d the efficiency grows and becomes stabilized, but $\eta_{3\text{–}fu} > \eta_{6\text{–}fu}$. Reprinted figure with permission from [48]. Copyright 2008 by the American Physical Society.

efficiency is very small, $\eta \to 0$, similar to the macroscopic electric motors [43]. These simulations have demonstrated that synthetic rotary molecular motors can have robust performance under load, and in the presence of noise and defects.

2.2. Molecular propellers

In recent years, there has been a large progress in the development of micro and nanoscale systems exploiting rotary motion in fluids. For example, Angelani *et al.* theoretically proposed a micromotor that unidirectionally rotates in a bath of bacteria [54], as shown in Figure 6. The system operates like a ratchet [34], which can provide unidirectional motion in the presence of both asymmetry and nonequilibrium. This theoretical scheme was experimental realized by Grzybowski *et al.*, who found that when gears with asymmetric teeth were positioned in aerobic bacteria *Bacillus subtilis* moving randomly in a fluid film, the gears were rotated unidirectionally [55]. The unidirectional rotation was observed only in the regime of collective bacterial swimming. The angular velocity of the gear was controlled by the amount of oxygen available to the bacteria.

In another example, colloidal magnetic microparticle chains connected by DNA molecules were powered by oscillatory magnetic fields to send sinusoidal waves toward their ends, in analogy to a flagellum [56]. Chains of magnetic microparticles [57], colloidal particles [58], and nanowires [59] were driven by magnetic fields in recent experiments. Zhang *et al.* has achieved continuous rotary motions of a nanoscale gold nanomotor with attached silica microdisk by optically exciting its plasmonic modes [60].

Today, nanoscale objects can be moved by AFM, light tweezers [61, 62], and other techniques. However, future nanosystems might need to move autonomously. In order to design nanoscale devices autonomously moving in

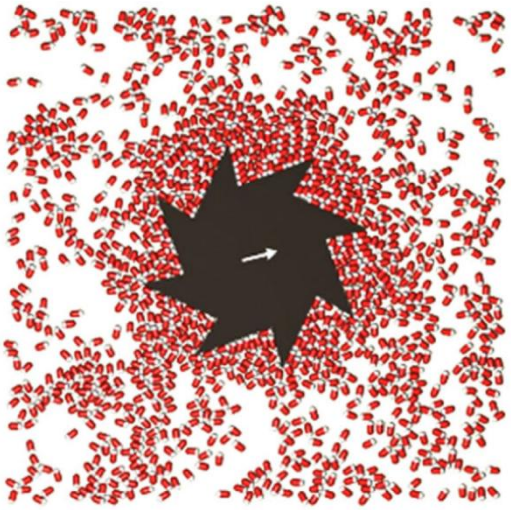

Figure 6. Simulation of an asymmetric rotor placed in a bath of bacteria. In the presence of asymmetry and nonequilibrium (bacteria), the rotor rotates in one direction. Reprinted figure with permission from [54]. Copyright 2009 by the American Physical Society.

liquids, we need to understand the physical laws that determine their motion. Flow of fluids around nanoscale structures is characterized by low Reynolds numbers (ratio of inertial and viscous forces), $R = av\rho/\eta$, where a is the size of the system, v its velocity, ρ its density and η is the viscosity of the fluid. In low-R environments, inertia is negligible, and viscosity dominates the motion of objects. According to "scallop theorem," systems can pump fluids and propel themselves in low Reynolds number conditions if their motion is not time reversible (it looks the same upon time reversal) [63]. Since unidirectional rotary motion is not time reversible, it is suitable for driving nanoscale machines in liquids. On the other hand, repetitive beating of rigid (molecular) structures is time reversible.

Nanoscale rotary machines can operate in configurations that are analogous to those used by macroscale systems. For example, Michl *et al.* studied molecular rotors and proposed that surface-mounted rotating molecules could operate in two modes, shown in Figure 7 [64]. Macroscale propellers convert rotary motion into thrust. Recently, we have studied by molecular dynamics (MD) simulations nanoscopic propellers in several configurations analogous to the macroscopic systems [65]. The propellers were formed by (8,0) carbon nanotubes (CNT) [49], with covalently attached and "chemically tunable" blades. These organic propellers or their analogs could potentially be synthesized by cyclic addition reactions [66]. We have designed two types of propellers: (1) the bulk propeller, shown in Figure 8 (top left), can pump liquid along the tube z-axis, due to two blades being tilted with respect to the nanotube axis; (2) the surface propeller, shown in Figure 8 (top right), pumps water orthogonal to the tube axis by four larger blades aligned straight along the axis.

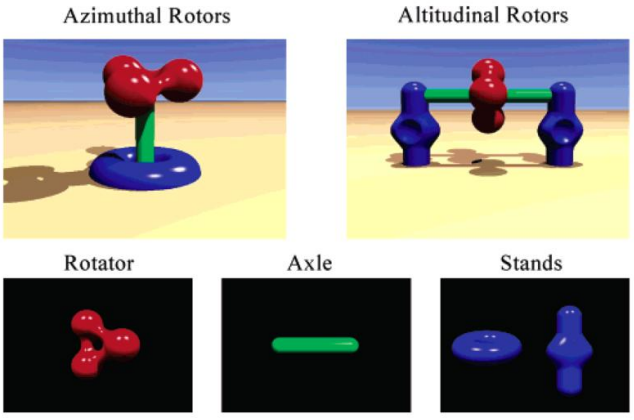

Figure 7. Schemes of surface-bound molecular rotors. Reprinted with permission from [64]. Copyright 2005 American Chemical Society.

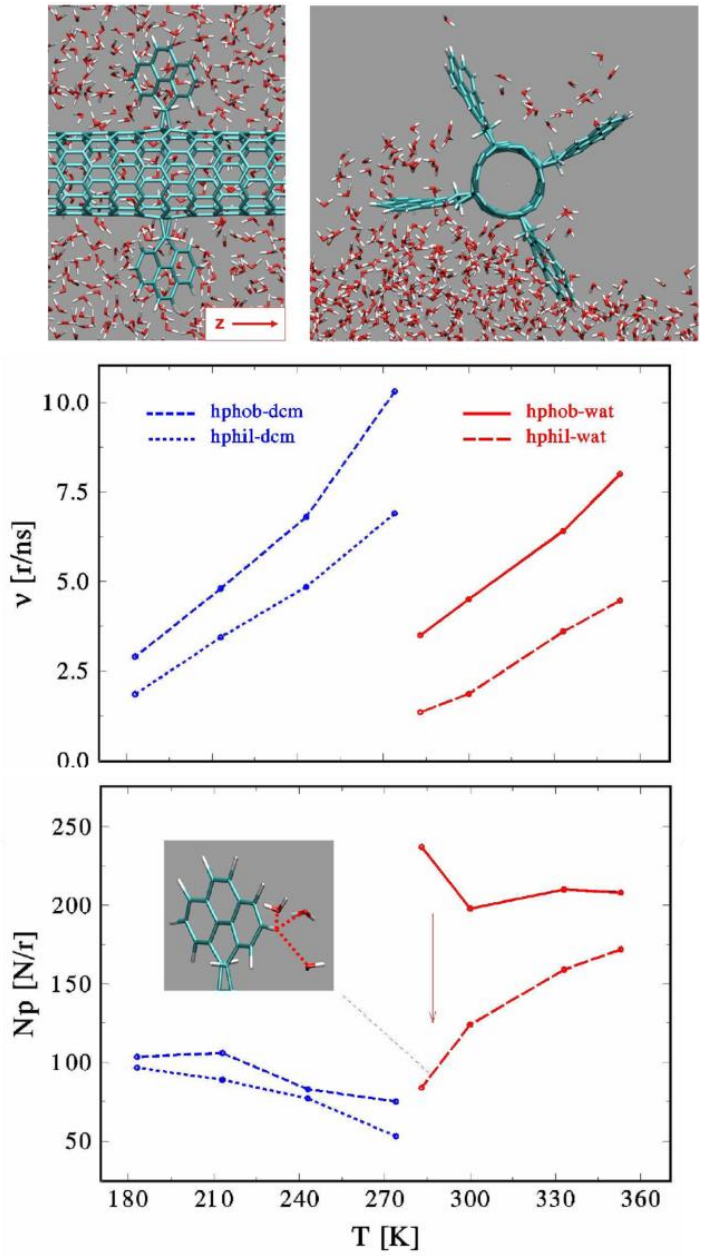

Figure 8. The bulk (top left) and surface (top right) water propellers that pump water along the tube (z) axis and orthogonal to it, respectively. (middle) Rotation rates (round/ns) of the bulk hydrophobic ("pho") and hydrophilic ("phi") propellers in water and DCM solvents as a function of temperature. (bottom) The pumping rates (molecules/round) of the bulk hydrophobic and hydrophilic propellers in water and DCM solvents as a function of temperature. (inset) Formation of hydrogen bonds between the hydrophilic blades and water can dramatically reduce the pumping rate. Reprinted figure with permission from [65]. Copyright 2007 by the American Physical Society.

We have demonstrated that these propellers can pump liquids when driven by constant applied torque on the CNT. Figure 8 shows the temperature dependence of the rotation rates (middle) and pumping rates (bottom) of the bulk hydrophobic and hydrophilic propellers with different blades, obtained in the hydrophobic dichloromethane (DCM) and hydrophilic water solvents. As the systems are heated above the (normal) freezing points of the solvents, T_f^{DCM}= 175 K and T_f^{water}= 273 K, their rotation rates grow, due to smaller solvent viscosities. The hydrophilic propeller rotates more slowly, since its polar blades interact more strongly with both solvents. Substantially slower rotation occurs in water that forms hydrogen bonds with its polar blades [67] (see inset in Figure 8).

The pumping rates in two solvents are significantly different, as seen in Figure 8 (bottom). In the DCM solvent, they are low due to the weak coupling between the solvent molecules and the blades. In the polar (water) solvent, water molecules form clusters, transiently held together by hydrogen bonds. This can effectively increase the cross section of the hydrophobic blades and the pumping rate, in agreement with Figure 8 (bottom). In the

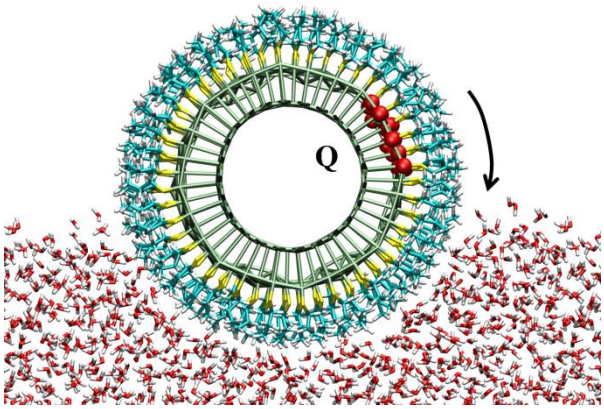

Figure 9. Model nanorod rolling on the water surface by optically induced asymmetric polarization of the chromophores and related Coulombic coupling to water. Reprinted figure with permission from [69]. Copyright 2009 by the American Physical Society.

hydrophilic propeller, water forms relatively stable hydration shells around the blades that reduce the effective space available for a direct contact of the pumped molecules with the blades. This can drastically decrease the pumping rates with respect to the hydrophobic propeller. At high temperatures, the hydrogen bonds break down and the pumping rates tend to be the same in both types of propellers.

These molecular propellers could be used as functional components of nanomachines. One can imagine that a nanomotor (the γ-subunit of the F_1 unit of the ATPase enzyme), driven by the ATP hydrolysis, can be linked to the molecular propellers described above. In this way, functional units capable of transporting nanoscale cargo could be prepared and operated in liquids.

2.3. Molecular rollers

One can also exploit micro and nanoscale systems that can perform autonomous motion on liquid surfaces. In lab-on-a-chip devices, droplets can be set in motion by dynamical electrowetting, where electrical fields generated by an array of electrodes act on the polar molecules and ions present in the droplets [68].

Recently, we explored by atomistic MD simulations [69] rolling of surfactant-covered nanorods on water surfaces by electric fields. In reality, the liquid rollers might be formed by nanorods covered with surfactants containing photoactive and partially oriented chromophores. The nanorods could be rotated by excitation of the chromophores with a light beam tilted with respect to the water surface. Coulombic attraction of the transiently and asymmetrically polarized or charged chromophores in the nanorods to the polar water molecules should cause unidirectional reorientation (rolling) of the nanorods.

In Figure 9, we show a model alkane-covered nanorod with an (empty) coarse-grained core that is locally and transiently charged on its surface. Driving of these model nanorods was simulated by adding small rechargeable electrodes on their surfaces: a narrow stripe of beads, positioned in the layer adjacent to the core and parallel to the water surface, is sequentially recharged (see Figure 9). We have tested two recharging regimes, where one stripe along the roller circumference is always homogeneously charged with one electron. In the "quasi-stochastic" regime, recharging of the stripe shifted counterclockwise by $\theta = \pi/6$ from the actually charged stripe was performed once its angle with the water surface drops below $\pi/6$. In the "periodic" regime, recharging of the next counterclockwise positioned stripe was realized periodically every t_C, giving a charged wave on the surface.

We have shown that with the proposed driving, nanorods with radii of $R_N = 2 - 5$ nm can roll on water with translational velocities of $v_{tran} = 1 - 5$ nm/ns [69]. The extent of coupling between rotational and translational motions is given by the efficiency of the rolling motion, defined as $S = v_{tran}/R_N\, v_{rot}$, where v_{rot} is the angular velocity. The efficiency, S, can be controlled by the chemistry at the nanorod-water interface. It turns out that translational velocities and efficiencies of the rolling motion depend on the coupling strength between surfactants and water, ε_s. In the ideal (non-slipping) system, $S \rightarrow 1$, while surfactant-covered nanorods roll on the dynamic water surface with greatly reduced efficiencies of $S = 0.1 - 0.4$. These simulations demonstrated that nanorods need to couple well to the water surface but not solvate in order to become propelled with minimal slipping during rotation [69].

3. Actuation in nanofluidics

Rotary motion could also be exploited in synthetic nanopores to control their selectivity and molecular passage rates. Current synthetic

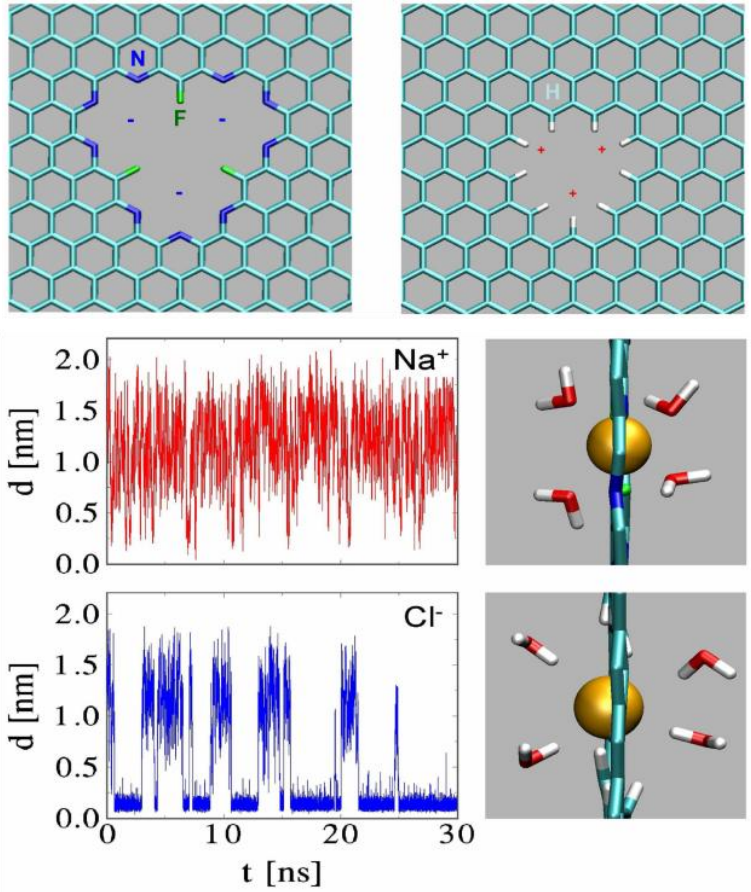

Figure 10. (top) Functionalized graphene nanopores. (left) The F–N-terminated nanopore. (right) The H-terminated nanopore. (bottom left) Time-dependent distance d between the Na^+ and Cl^- ions and the centers of the F–N-pore and H-pore, respectively, at the field of E = 6.25 mV/nm. The dynamics of passage of these ions through the two pores is very different. (bottom right) While both ions are surrounded by two water half-shells, when passing through their pores, only the Cl^- ion has relatively stable binding to the H–pore. Reprinted with permission from [77]. Copyright 2008 American Chemical Society.

nanopores are based on inorganic materials, such as zeolites [70], carbon [71] or silica [72]. Future synthetic nanopores can be based on novel proteins [73–76]. Such nanopores could be similar to channel proteins, formed by precisely arranged sequences of amino acids that can efficiently recognize and guide the passing molecular species. Below, we describe recently designed molecular nanopores, where rotary motion was implemented.

3.1. Graphene nanopores

First, we discuss how selective molecular passage can be realized in porous nanocarbons [77]. Recently, we have modeled by MD simulations the passage of ions through functionalized nanopores formed in graphene monolayers [77]. In Figure 10 (top), we display the studied pores with diameter of $d \sim 5$ Å, terminated by either negatively charged nitrogens and fluorines (left) or by positively charged hydrogens (right).

In Figure 10 (bottom right), we show the configurations of the Na^+ and Cl^- ions passing through the two nanopores. The polar and charged nanopore rim can replace several water molecules from the first hydration shell of the ion passing through it. Therefore, the passing ion is surrounded by two separated (incomplete) hydration "half-shells" at both sides. Since the contact between the ions and the pore rims can be very tight, the pores could be made highly selective.

Figure 10 (bottom left) displays the time-dependent distance d between the ions and their pore centers, obtained at a low field of E = 6.25 mV/nm. The distance fluctuations reveal very different dynamics in the two cases. The Na^+ ion passes the F–N-pore fast, without significantly binding with it. The ion rarely gets closer than 5 Å to the pore center and stays most of the time in the water region (d > 10 Å). Simulations show that the K^+ ion passes more easily than the Na^+ ion through this pore, due to its weaker binding to the hydration shell. The Cl^- ion has even more stable binding to the symmetric H-pore, where it stays for ~ 70% of the time. Recent theoretical and experimental studies also indicate that porous graphene could serve as a sieve of high selectivity and transparency, potentially useful in DNA sequencing [78].

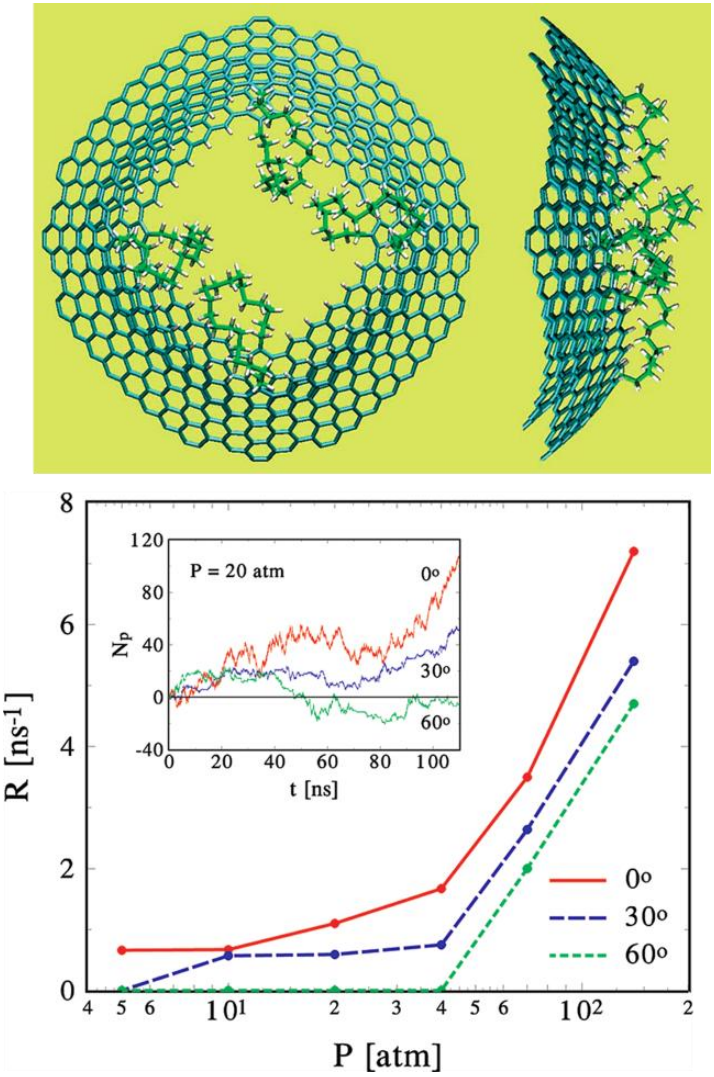

Figure 11. (top) The stacked (untwisted) pair of nanocones. (bottom) Dependence of the rate of pentane flow through the nanopore on the applied pressures, at rotation angles of θ_{rot} = 0°, 30° and 60°. (inset) The time dependence of total number of pentane molecules that pass the nanopore N_p, at the applied pressure of P = 20 atm and different θ_{rot}. Reprinted with permission from [79]. Copyright 2010 American Chemical Society.

3.2. Molecular nanovalve

We have extended the above ideas by connecting two carbonaceous pores with functional ligands. The selectivity and passage rates of these hybrid pores can be controlled by mutual rotation of the carbonaceous components [79].

In Figure 11 (top), we show two carbon nanocones that are stacked and covalently connected by aliphatic chains at their open tips, in analogy to aquaporins. The functionality of this nanovalve structure is based on the fact that the size of the nanopore is altered when one nanocone is gradually rotated with respect to the other. If we mutually rotate them by a certain angle θ_{rot}, the aliphatic chains become stretched, helically wrapped, and entangled inside the nanopore. The rotation of nanocones is precise and reproducible, due to π–π stacking of the cones.

In Figure 11 (bottom), we plot the flow rate, R, of pentane through the hybrid pore in dependence on the pressure, P, at θ_{rot} = 0°, 30° and 60°. At θ_{rot} = 0°, the cone is opened, R grows with pressure, and it is nonzero even at small pressures. As the angle is increased to θ_{rot} = 30°, the flow becomes smaller at low pressures. At θ_{rot} = 60°, there is practically no pentane flow up to P = 40 atm.

In the inset of Figure 11 (bottom), we also show the time dependence of the total number of pentanes that pass the nanopore at P = 20 atm. The size of the time-dependent fluctuations in N_p reflects fluctuations in the sizes of the nanopore, caused by the alkyl chains that rotate and change their conformations. For more closed pores, the fluctuations of N_p are smaller, due to stretched alkyl chains.

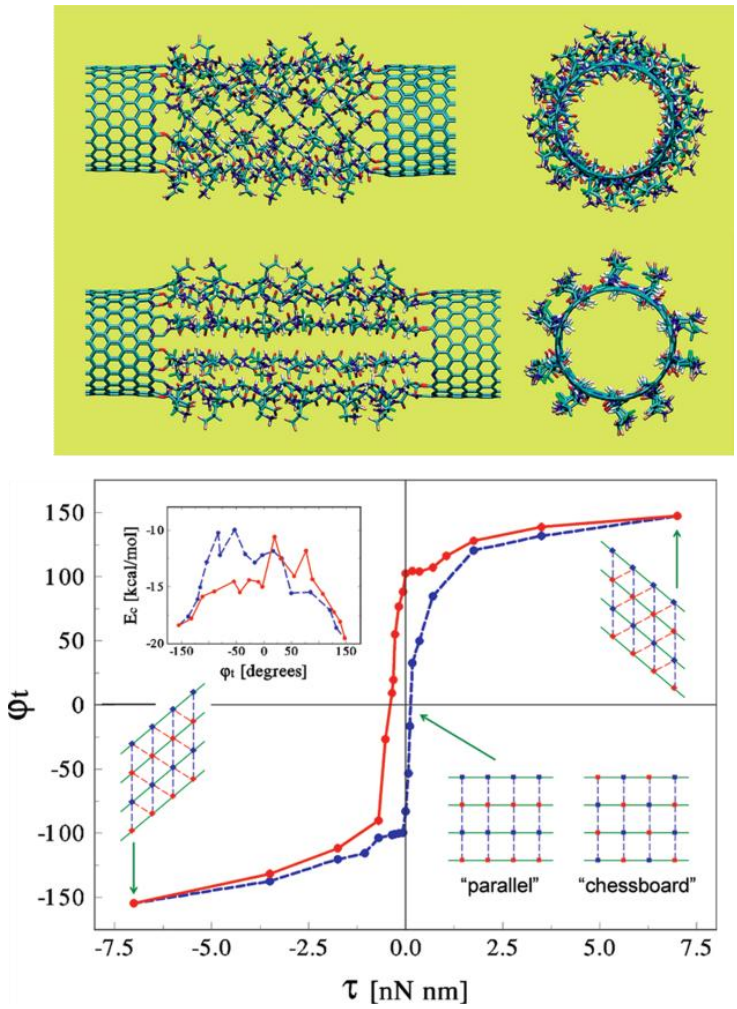

Figure 12. (top) Two types of 12-residue hybrid nanochannels solvated in water at T = 300 K. (bottom) The twist angle-torque hysteresis curve obtained in one cycle for the parallel 8-residue structure. Additional schemes show the charges and their mutual coupling in the straight and twisted structures. (inset) The related Coulombic energy-twist angle hysteresis curve. Reprinted with permission from [79]. Copyright 2010 American Chemical Society.

3.3. Biomimetic ammonia switch

We can use rotary motion to also control the selectivity of the synthetic nanopores. In Figure 12 (top), we show hydrated nanopores formed by carbon nanotubes joined with cylindrical structures of antiparallel peptide chains, forming a barrel similar to those present in certain proteins (GFP). We have tested two types of nanopores, where one is more stable in any of the two possible twisted forms, due to the arrangement of the charged groups, while the other is more stable in the straight form (see Figure 12 (top)). Rotation of one CNT with respect to the other in the system that is more stable when twisted (discussed below) results in the formation of either forward or backward-twisted peptide barrels.

In Figure 12 (bottom), we present the hysteresis curve for the dependence of the twist angle on the torque applied to the parallel 8-residue nanopore. The results are obtained in one twisting trajectory going between the two end points (wrapped cylinders) and back, where each data point is averaged over 1,000 frames separated by 100 fs, after equilibration for 1 ns. The hysteresis curve shows that the nanopore can be stabilized in two configurations with non-zero twist angles, upon removal of the torque.

These hybrid nanochannels are highly tunable due to a large selection of amino acids that can coat the inner channel walls. By screening the amino acid residues inside the peptide barrel, we have identified those which can make the channel interior selective to passage of NH_3 (ammonia) molecule. In particular, we have found a system that allows the passage of ammonia in one twisted configuration but it blocks it in the other configuration. In Figure 13 (top), we show the interior of this peptide channel, containing two tryptophan (TRP) and two tyrosine (TYR) residues, obtained for the two opposite twists.

In Figure 13 (bottom), we plot the number N_p of NH_3 molecules passed under

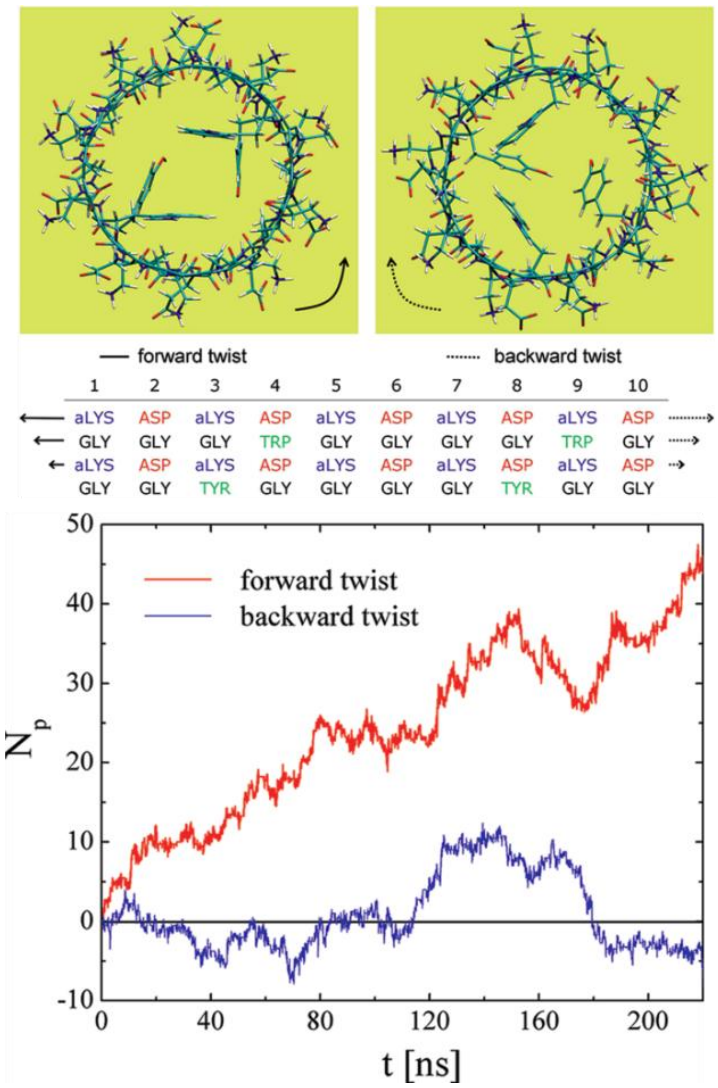

Figure 13. (top) Axial view of the two twisted configurations of the parallel 4-residue 10-peptide junction, with 2 tryptophan and 2 tyrosine residues in its interior. (middle) Amino acid sequence map of 4-residue 10-peptide junction. Each column corresponds to a peptide chain, and the odd/even rows are residues with sidechains that are exposed outwards/inwards. (bottom) The time dependence of the total number N_p of NH_3 molecules passed through the twisted nanochannels. Reprinted with permission from [79]. Copyright 2010 American Chemical Society.

steady-state conditions through these channels within the simulation time *t*. The results show dramatically different flow rates, $R_{NH3} = N_p/t \sim 0.18$ and ~ 0, for the forward and backward twisted configurations of the channel, respectively. In the forward twist, two pairs of interior residues shadow each other, thus increasing the cross section area available for the NH_3 passage. In the backward twist, the TRP and TYR residues are spread around the circumference of the channel, thus reducing the cross section area available for the NH_3 passage. These results demonstrate that the highly tunable barrel junction can act as a mechanical switch for the flow of selected molecules.

4. Self-assembly of nanocarbons

We may also induce, guide, and control the self-assembly of nanoscale materials of different shapes, interactions, and properties. Carbon allotropes [80], such as graphene [81–90], can be prepared in many sizes, types, and chemically distinct forms. For example, graphene nanoribbons (GNR) have been synthesized [29, 91–93], and etched by lithographic [94, 95] and catalytic methods [96–98]. Graphene flakes with strong interlayer van der Waals (vdW) coupling and chemical functionalization can self-assemble into larger structures [99–101]. Individual flakes with high elasticity [102–104] could fold into a variety of 3D structures [105], such as carbon nanoscrolls [106–109].

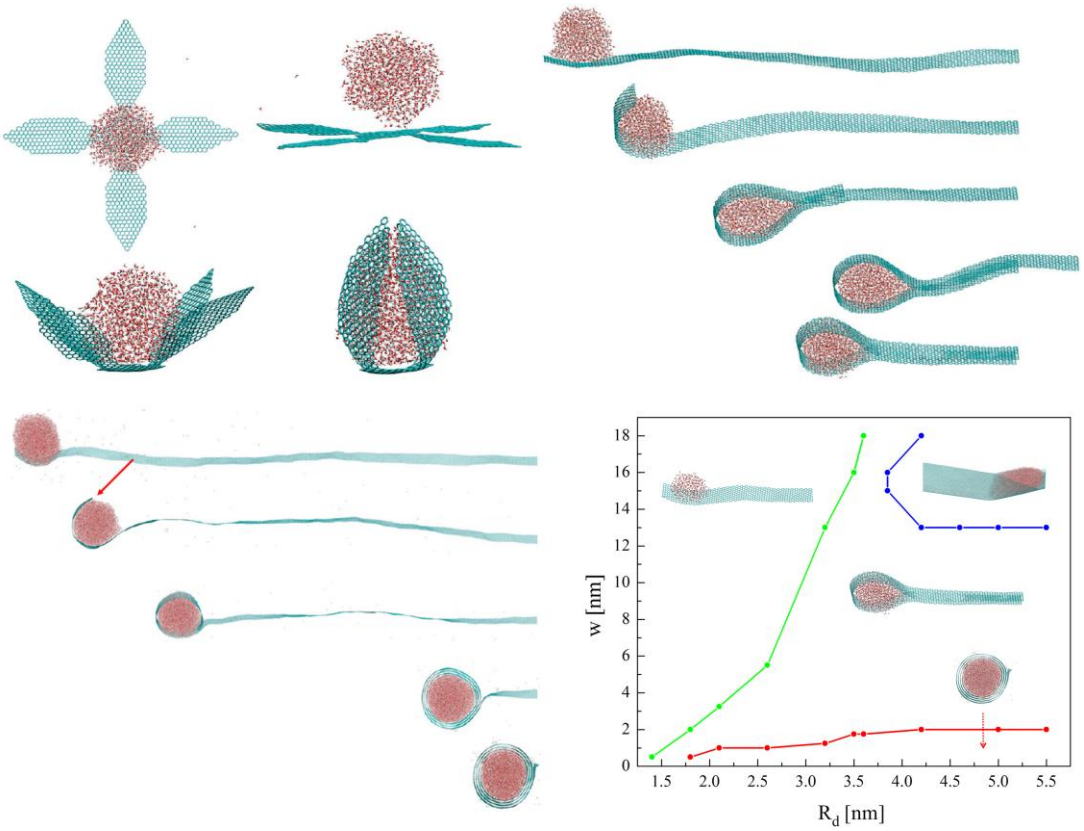

Figure 14. (top left) ND-assisted folding of a star-shaped graphene flake. (top right) Folding and sliding of a GNR (30 × 2 nm^2), activated and guided by a ND with N_w = 1,300 waters and the radius of R_d ~ 2.1 nm. (bottom left) Folding and rolling of a GNR (90 × 2 nm^2) by ND with N_w = 10, 000 waters and the radius of R_d ~ 4.2 nm. (bottom right) The phase diagram of GNR folding by water NDs. We can see the nonfolding, sliding, rolling, and zipping phases. Reprinted with permission from [110]. Copyright 2009 American Chemical Society.

4.1. Droplet-driven self-assembly of graphene

Recently, we have studied how planar graphene flakes of different shapes and sizes can be activated and guided to self-assemble into 3D-nanostructures [110]. We have shown that water nanodroplets (ND) can induce rapid bending, folding, sliding, rolling, and zipping of graphene flakes, leading to nanoscale sandwiches, capsules, knots, and rings.

In Figure 14 (top left), we show that once a ND with N_w = 1, 300 water molecules is placed at T = 300 K above a star-shaped flake, the droplet binds by vdW coupling to the flake and induces its bending and closing, within t ~ 1 ns. NDs can also induce folding of GNRs. As shown in Figure 14 (top right), when a ND (N_w = 1300) is positioned above the free end of the GNR (30 × 2 nm^2), the free end folds into a knot structure, touches the ribbon surface, and starts to slide fast on it due to strong vdW binding. When the radius of ND is several times larger than the graphene width, it induces the formation of a multilayer ring structure, similar to multiwall carbon nanotubes, as seen in Figure 14 (bottom left). In Figure 14 (bottom right), we summarize the observed nanostructures obtained in the self-assembly of GNRs of the width of w and the water droplet of the radius of R_d. When $R_d > w$ the nanodroplets can activate and guide better the GNR self-assembly. Experimentally, the droplets could be deposited on graphene by Dip-Pen nanolithography [111] or AFM [112].

4.2. Nanotube-driven self-assembly of graphene

We have also tested if CNTs and other nanoscale materials could activate and guide the self-assembly of GNRs on their surfaces and in their interiors [113]. In Figure 15, we present the results of our MD simulations of the CNT-assisted GNR self-assembly at T = 300 K. The (a-c) insets show the self-assembly of the GNR (40×3 nm^2) once placed on the surface of (60,0) CNT (with two ends fixed). The (d-e) insets shows the self-assembly of this GNR inside the same CNT. The (f) inset shows that two GNRs (40 × 1 nm^2) can self-assemble into a double helix inside the same CNT. In the above described manner, one could in principle assemble arbitrary planar graphene nanostructures on the surfaces or in the interiors of CNTs [113].

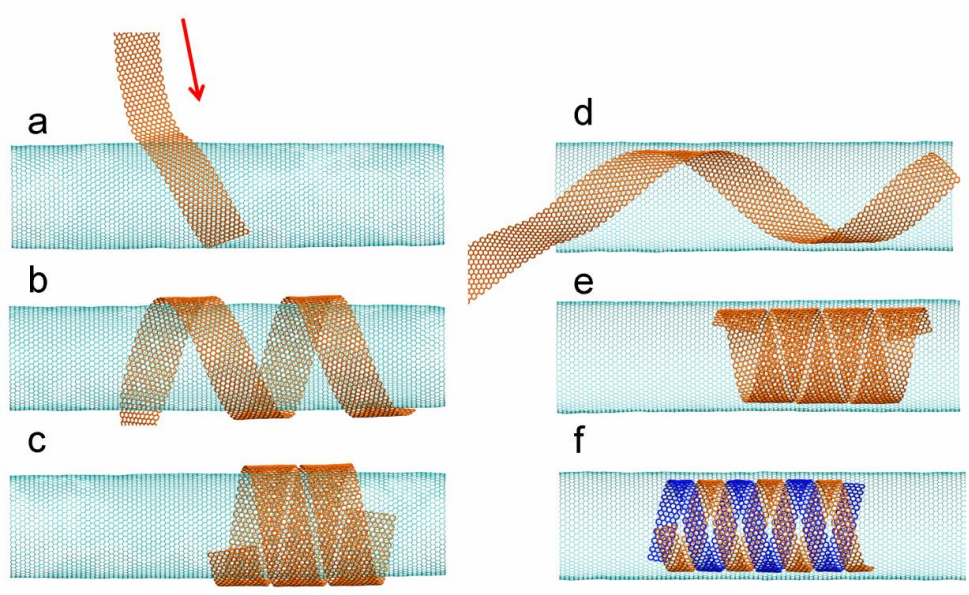

Figure 15. (a-c) Folding and rolling of a GNR with the size of 40 × 3 nm^2, when it is placed at the angle of 60° with respect to the axis of the (60,0) CNT. (d-e) Folding and rolling of this GNR when it is placed inside this CNT (front part of the CNT is removed for better visualisation). (f) Folding and rolling of two GNRs (40 × 1 nm^2) placed inside this CNT. From [113].

5. Conclusions

In summary, we have shown that control of rotary motion can be used in the preparation and activation of functional nanosystems. We discussed implementation of these principles in molecular motors, propellers, and wheels rolling on liquids. We have also shown how inorganic and biomimetic channels can be designed to serve as molecular switches, where mutual rotation of the individual components can control or selectively block the flow of different molecules. Finally, we have demonstrated that one could control the self-assembly of graphene nanostructures realized with the help of nanodroplets and graphene nanotubes. These studies can lead to the construction of new building blocks in functional nanodevices, with unique mechanical, electrical, or optical properties, finding applications in electronics, sensing, and medicine.

Acknowledgements

This work was partially supported by a grant from NSF (CBET-0932812). The calculations have been realized with the NERSC, NCSA and CNM supercomputer networks.

References

1. T. Atsumi, L. McCarter, T. Imae, Nature 355 (1992) 182.
2. C. Brennen, H. Winet, Annu. Rev. Fluid Mech. 9 (1977) 339.
3. A. Aksimentiev, I. A. Balabin, R. H. Fillingame, K. Schulten, Biophys. J. 86 (2004) 1332.
4. R. Bru, A. Sanchez-Ferrer, F. Garcia-Carmona, Biochem. J 310 (1995) 721.
5. R. D. Valle, R. A. Milligan, Science 288 (2000) 88.
6. A. Gennerich, R. D. Valle, Curr. Opin. Cell Biol. 21 (2009) 59.
7. J. S. Bergs, B. C. Powell, R. E. Cheney, Mol. Biol. Cell 12 (2001) 780.
8. R. K. Soong, G. D. Bachand, H. P. Neves, A. G. Olkhovets, H. G. Craighead, C. D. Montemagno, Science 290 (2000) 1555.
9. C. Brunner, C. Wahnes, V. Vogel, Lab Chip 7 (2007) 1263.
10. A. Goel, V. Vogel, Nat. Nanotechnol. 3 (2008) 465.
11. M. G. L. van den Heuvel, C. Dekker, Science 317 (2007) 333.
12. S. Iijima, Nature 354 (1991) 56.
13. M. S. Dresselhaus, G. Dresselhaus, P. C. Eklund, Science of Fullerenes, Carbon Nanotubes, Academic Press Inc., San Diego (1996).
14. K. S. Novoselov, A. K. Geim, S. V. Morozov, D. Jiang, Y. Zhang, S. V. Dubonos, I. V. Grigorieva, A. A. Firsov, Science 306 (2004) 666.
15. M. Zheng, A. Jagota, M. S. Strano, A. P. Santos, P. Barone, S. G. Chou, B. A. Diner, M. S. Dresselhaus, R. S. Mclean, G. B. Onoa, G. G. Samsonidze, E. D. Semke, M. Usrey, D. J. Walls, Science 302 (2003) 1545.

16. S. Stankovich, D. A. Dikin, G. H. B. Dommett, K. M. Kohlhaas, E. J. Zimney, E. A. Stach, R. D. Piner, S. T. Nguyen, R. S. Ruoff, Nature 442 (2006) 282.
17. S. Banerjee, T. Hemraj-Benny, S S. Wong, Adv. Mater. 17 (2005) 17.
18. F. Cervantes-Sodi, G. Csanyi, S. Piscanec, A. C. Ferrari, Phys. Rev. B. 77 (2008) 165427.
19. D. W. Boukhvalov, M. I. Katsnelson, Nano Lett. 8 (2008) 4373.
20. S. Ferro, A. De Battisti, Anal. Chem. 75 (2003) 7040.
21. D. A. Dikin, S. Stankovich, E. J. Zimney, R. D. Piner, G. H. B. Dommett, G. Evmenenko, S. T. Nguyen, R. S. Ruoff, Nature 448 (2007) 457.
22. W. Cai, R. D. Piner, F. J. Stadermann, S. Park, M. A. Shaibat, Y. Ishii, D. Yang, A. Velamakanni, S. J. An, M. Stoller, J. An, D. Chen, R. S. Ruoff, Science 321 (2008) 1815.
23. A. M. Fennimore, T. D. Yuzvinsky, W.-Q. Han, M. S. Fuhrer, J. Cumings, A. Zettl, Nature 424 (2003) 408.
24. B. Bourlon, D. C. Glattli, C. Miko, L. Forro, A. Bachtold, Nano Lett. 4 (2004) 709.
25. S. W. D. Bailey, I. Amanatidis, C. J. Lambert, Phys. Rev. Lett. 100 (2008) 256802.
26. J. E. Green, J. W. Choi, A. Boukai, Y. Bunimovich, E. Johnston-Halperin, E. DeIonno, Y. Luo, B. A. Sheriff, K. Xu, Y. S. Shin, H.-R. Tseng, J. F. Stoddart, J. R. Heath, Nature 445 (2007) 414.
27. P. Král, H. R. Sadeghpour, Phys. Rev. B 65 (2002) 161401.
28. J. Plewa, E. Tanner, D. M. Mueth, D. G. Grier, Opt. Express 12 (2004) 1978.
29. S. Tan, H. A. Lopez, C. W. Cai, Y. Zhang, Nano Lett. 4 (2004) 1415.
30. J. Vacek, J. Michl, Proc. Natl. Acad. Sci. U.S.A. 98 (2001) 5481.
31. P. Král, T. Seideman, J. Chem. Phys. 123 (2005) 184702.
32. T. R. Kelly, H. De Silva, R. A. Silva, Nature 401 (1999) 150.
33. A. Barreiro, R. Rurali, E. R. Hern´andez, J. Moser, T. Pichler, L. Forr´o, A. Bachtold, Science 320 (2008) 775.
34. R. D. Astumian, Science 276 (1997) 917.
35. J. L. Bull, A. J. Hunt, E. Meyhöfer, Biomed. Microdev. 7 (2005) 21.
36. T. R. Kelly, X. Cai, F. Damkaci, S. B. Panicker, B. Tu, S. M. Bushell, I. Cornella, M. J. Piggott, R. Salives, M. Cavero, Y. Zhao, S. Jasmin, J. Am. Chem. Soc. 129 (2007) 376.
37. N. Koumura, R. W. J. Zijlstra, R. A. van Delden, N. Harada, B. L. Feringa, Nature 401 (1999) 152.
38. J.-F. Morin, Y. Shirai, J. M. Tour, Org. Lett. 8 (2006) 1713.
39. Y. Shirai, A. J. Osgood, Y. Zhao, K. F. Kelly, J. M. Tour, Nano Lett. 5 (2005) 2330.
40. J. K. Gimzewski, C. Joachim, R. R. Schlittler, V. Langlais, H. Tang, I. Johannsen, Science 281 (1998) 531.
41. L. Grill, K. H. Rieder, F. Moresco, G. Rapenne, S. Stojkovic, X. Bouju, C. Joachim, Nat. Nanotechnol. 2 (2007) 95.
42. G. Vives, H.-P. J. de Rouville, A. Carella, J.-P. Launay, G. Rapenne, Chem. Soc. Rev. 38 (2009) 1551.
43. H. Auinger, Power Eng. J. 15 (2001) 163.
44. G. Rapenne, Org. Biomol. Chem. 3 (2005) 1165.
45. A. Carella, G. Rapenne, J.-P. Launay, New J. Chem. 29 (2005) 288.
46. H. Park, J. Park, A. K. L. Lim, E. H. Anderson, A. P. Alivisatos, P. L. McEuen, Nature 407 (2000) 57.
47. C. C. Kaun, T. Seideman, Phys. Rev. Lett. 94 (2005) 226801.
48. B. Wang, L. Vuković, P. Král, Phys. Rev. Lett. 101 (2008) 186808.
49. J. Han, A. Globus, R. Jaffe, G. Deardorff, Nanotechnology 8 (1997) 95.
50. J. Cumings, A. Zettl, Science 289 (2000) 602.
51. C. A. Cupas, L. Hodakowski, J. Am. Chem. Soc. 96 (1974) 4668.
52. K. V. Mikkelsen, M. A. Ratner, Chem. Rev. 87 (1987) 113.
53. P. Král, Phys. Rev. B 56 (1997) 7293.
54. L. Angelani, R. D. Leonardo, G. Ruocco, Phys. Rev. Lett. 102 (2009) 048104.
55. A. Sokolova, M. M. Apodaca, B. A. Grzybowski, I. S. Aranson, Proc. Natl. Acad. Sci. U.S.A. 107 (2009) 969.
56. R. Dreyfus, J. Baudry, M. L. Roper, M. Fermigier, H. A. Stone, J. Bibette, Nature 437 (2005) 862.
57. A. Snezhko, M. Belkin, I. S. Aranson, W.-K. Kwok, Phys. Rev. Lett. 102 (2009) 118103.
58. P. Tierno, R. Golestanian, I. Pagonabarraga, F. Sagu´es, Phys. Rev. Lett. 101 (2008) 218304.
59. K. Keshoju, H. Xing, L. Sun, Appl. Phys. Lett. 91 (2007) 123114.
60. M. Liu, T. Zentgraf, Y. Liu, G. Bartal, X. Zhang, Nat. Nanotechnol. 5 (2010) 570.
61. A. Ashkin, J. M. Dziedzic, J. E. Bjorkholm, S. Chu, Opt. Lett. 11 (1986) 288.
62. R. E. Holmlin, M. Schiavoni, C. Y. Chen, S. P. Smith, M. G. Prentiss, G. M. Whitesides, Angew. Chem. Int. Ed. 39 (2000) 3503.
63. E. M. Purcell, Am. J. Phys. 45 (1977) 3.
64. G. S. Kottas, L. I. Clarke, D. Horinek, J. Michl, Chem. Rev. 105 (2005) 1281.

65. B. Wang, P. Král, Phys. Rev. Lett. 98 (2007) 266102.
66. D. Tasis, N. Tagmatarchis, A. Bianco, M. Prato, Chem. Rev. 106 (2006) 1105.
67. K. A. T. Silverstein, A. D. J. Haymet, K. A. Dill, J. Am. Chem. Soc. 122 (2000) 8037.
68. M. Abdelgawad, A. R. Wheeler, Adv. Mater. 21 (2009) 920.
69. L. Vuković, P. Král, Phys. Rev. Lett. 103 (2009) 246103.
70. E. Jordan, R. G. Bell, D. Wilmer, H. Koller, J. Am. Chem. Soc. 128 (2006) 558.
71. S. M. Saufi, A. F. Ismail, Carbon 42 (2004) 241.
72. M. C. Duke, J. C. D. da Costa, D. D. Do, P. G. Gray, G. Q. Lu, Adv. Funct. Mater. 16 (2006) 1215.
73. Z. Qi, M. Sokabe, K. Donowaki, M. Ishida, Biophys. J. 76 (1999) 631.
74. B. Kuhlman, G. Dantas, G. C. Ireton, G. Varani, B. L. Stoddard, D. Baker, Science 302 (2003) 1364.
75. J. Kaplan, W. F. DeGrado, Proc. Natl. Acad. Sci. U.S.A. 101 (2004) 11566.
76. C.-J. Tsai, J. Zheng, R. Nussinov, PLoS Comput. Biol. 2 (2006) e42.
77. K. Sint, B. Wang, P. Král, J. Am. Chem. Soc. 130 (2008) 16448.
78. S. Garaj, W. Hubbard, A. Reina, J. Kong, D. Branton, J. A. Golovchenko, Nature 467 (2010) 190.
79. A. V. Titov, B. Wang, K. Sint, P. Král, J. Phys. Chem. B 114 (2010) 1174.
80. A. Hirsch, Nat. Mater. 9 (2010) 868.
81. K. S. Novoselov, A. K. Geim, S. V. Morozov, D. Jiang, Y. Zhang, S. V. Dubonos, I. V. Grigorieva, A. A. Firsov, Science 306 (2004) 666.
82. A. K. Geim, K. S. Novoselov, Nat. Mater. 6 (2007) 183.
83. S. Berner, M. Corso, R. Widmer, O. Groening, R. Laskowski, P. Blaha, K. Schwarz, A. Goriachko, H. Over, S. Gsell, M. Schreck, H. Sachdev, T. Greber, J. Osterwalder, Angew. Chem. Int. Ed. 46 (2007) 5115.
84. R. Laskowski, P. Blaha, T. Gallauner, K. Schwarz, Phys. Rev. Lett. 98 (2007) 106802.
85. G. Tsoukleri, J. Parthenios, K. Papagelis, R. Jalil, A. C. Ferrari, A. K. Geim, K. S. Novoselov, C. Galiotis, Small 5 (2009) 2397.
86. R. Balog, B. Jorgensen, L. Nilsson, M. Andersen, E. Rienks, M. Bianchi, M. Fanetti, E. Laegsgaard, A. Baraldi, S. Lizzit, Z. Sljivancanin, F. Besenbacher, B. Hammer, T. G. Pedersen, P. Hofmann, L. Hornekaer, Nat. Mater. 9 (2010) 315.
87. X. Yan, X. Cui, B. Li, L.-s. Li, Nano Lett. 10 (2010) 1869.
88. T. Cohen-Karni, Q. Qing, Q. Li, Y. Fang, C. M. Lieber, Nano Lett. 10 (2010) 1098.
89. Y. Wang, Y. Shao, D. W. Matson, J. Li, Y. Lin, ACS Nano 4 (2010) 1790.
90. P. Matyba, H. Yamaguchi, G. Eda, M. Chhowalla, L. Edman, N. D. Robinson, ACS Nano 4 (2010) 637.
91. L. Jiao, L. Zhang, X. Wang, G. Diankov, H. Dai, Nature 458 (2009) 877.
92. N. W. Shi Kam, T. C. Jessop, P. A. Wender, H. Dai, J. Am. Chem. Soc. 126 (2004) 6850.
93. D. V. Kosynkin, A. L. Higginbotham, A. Sinitskii, J. R. Lomeda, A. Dimiev, B. K. Price, J. M. Tour, Nature 458 (2009) 872.
94. L. Tapaszto, G. Dobrik, P. Lambin, L. P. Biro, Nat. Nanotechnol. 3 (2008) 397.
95. C. Stampfer, J. Göttinger, S. Hellmüller, F. Molitor, K. Ensslin, T. Ihn, Phys. Rev. Lett. 102 (2009) 056403.
96. L. Ci, Z. Xu, L. Wang, W. Gao, F. Ding, K. F. Kelly, B. I. Yakobson, P. M. Ajayan, Nano Res. 1 (2008) 116.
97. L. C. Campos, V. R. Manfrinato, J. D. Sanchez-Yamagishi, J. Kong, P. Jarillo-Herrero, Nano Lett. 9 (2009) 2600.
98. K. Kim, A. Sussman, A. Zettl, ACS Nano 4 (2010) 1362.
99. Z. Zhu, D. Su, G. Weinberg, R. Schlogl, Nano Lett. 4 (2004) 2255.
100. W. Jin, T. Fukushima, M. Niki, A. Kosaka, N. Ishii, T. Aida, Proc. Natl. Acad. Sci. U.S.A. 102 (2005) 10801.
101. Q. Chen, T. Chen, G.-B. Pan, H.-J. Yan, W.-G. Song, L.-J. Wan, Z.-T. Li, Z.-H. Wang, B. Shang, L.-F. Yuan, J.-L. Yang, Proc. Natl. Acad. Sci. U.S.A. 105 (2008) 16849.
102. C. Lee, X. Wei, J. W. Kysar, J. Hone, Science 321 (2008) 385.
103. J. S. Bunch, S. S. Verbridge, J. S. Alden, A. M. van der Zande, J. M. Parpia, H. G. Craighead, P. L. McEuen, Nano Lett. 8 (2008) 2458.
104. C. Gomez-Navarro, M. Burghard, K. Kern, Nano Lett. 8 (2008) 2045.
105. K. V. Bets, B. I. Yakobson, Nano Res. 2 (2009) 161.
106. L. M. Viculis, J. J. Mack, R. B. Kaner, Science 299 (2003) 1361.
107. S. F. Braga, V. R. Coluci, S. B. Legoas, R. Giro, D. S. Galv˜ao, R. H. Baughman, Nano Lett. 4 (2004) 881.
108. D. Yu, F. Liu, Nano Lett. 7 (2007) 3046.
109. A. Sidorov, D. Mudd, G. Sumanasekera, P. J. Ouseph, C. S. Jayanthi, S.-Y. Wu, Nanotechnology 20 (2009) 055611.
110. N. Patra, B. Wang, P. Král, Nano Lett. 9 (2009) 3766.

111. K.-B. Lee, S.-J. Park, C. A. Mirkin, J. C. Smith, M. Mrksich, Science 295 (2002) 1702.
112. A.-S. Duwez, S. Cuenot, C. Jerome, S. Gabriel, R. Jerome, S. Rapino, F. Zerbetto, Nat. Nanotechnol. 1 (2006) 122.
113. N. Patra, Y. Song, P. Král, ACS Nano 5 (2011) 1798.